Characterization and Application of Nanomaterials (2021) Volume 4 Issue 1
doi:10.24294/can.v4i1.1328

ORIGINAL RESEARCH ARTICLE

Influence of flow rate on the transport of $nTiO_2$ and phosphate and its modeling

Gang Feng[1,2], Nan Xu[1,2*], Zuling Li[1,2], Yuhe Cao[1,2], Keqing Sun[1,2]

[1]*School of Chemistry, Biology and Material Engineering, Suzhou University of Science and Technology, Suzhou 215009, China. E-mail: nanxu@mail.usts.edu.cn*

[2]*Jiangsu Key Laboratory of Environmental Functional Material, Suzhou 215009, China*

ABSTRACT

We studied Zeta potentials of nanoparticles titanium dioxides ($nTiO_2$) in different concentration of $NaNO_3$ and phosphate (P) solutions. In addition, the effect of flow rate on the transport of $nTiO_2$ in P was investigated at pH = 6.5. Experimental results show that the Zeta potential of $nTiO_2$ is compressed with the increasing ion concentration (IC) of $NaNO_3$ at pH = 6.5. The negative charge increases with the augment of P. Therefore, the high P and low $NaNO_3$ induce the stabilization of $nTiO_2$ aggregates. The transport experiments suggest that the rapid flow rate is favorable for the transportability of $nTiO_2$ and soluble phosphate. The breakthrough transport curves (BTCs) of $nTiO_2$ in sand columns can be fitted well with two-site kinetic attachment model. The modeling results suggest that the values of first-order attachment rate coefficients (k_2) and detachment rate coefficients (k_{2d}) on site 2 and first-order attachment rate coefficients (k_1) on site 1 are responsible to the attaching efficiency of $nTiO_2$ on sands and their transportability.

Keywords: $nTiO_2$; Zeta Potential; Transport; Phosphate

ARTICLE INFO

Received: 14 January 2021
Accepted: 28 February 2021
Available online: 6 March 2021

Nano titanium dioxide ($nTiO_2$) is one of the mass-produced metal oxide nano materials. Due to the ultra-high photocatalytic ability of nano materials, it has been more and more used in various fields and commercial products[1–5]. In mass production and wide application, some $nTiO_2$ cannot be avoided to be released into natural water and soil environment. A large amount of evidence shows that after artificial $nTiO_2$ enters the water body, it has adverse effects on aquatic organisms, including microorganisms, algae, invertebrates and fish[6,7]. Therefore, the study of the relationship between nanoparticles attached to soil saturated particles and nanoparticles in soil particle saturated porous media has become a hot spot in the study of the environmental behavior of nanoparticles. At present, the artificial nano materials studied internationally are mainly industrial fullerene nC_{60}, carbon nanotubes and silica nanoparticles. The mobility of these nano materials in saturated porous media is different. The flow rate of solution, ion concentration and surface potential of nanoparticles will affect their migration behavior[8,9]. Therefore, it is necessary to explore the changes of surface properties of $nTiO_2$ under different environmental conditions and its migration in the natural world. In agricultural production and people's life and production, a large number of phosphorus containing substances are used, which makes phosphorus containing substances enter into

soil and water. $nTiO_2$ particles have certain adsorption on phosphate, which changes its surface properties, and finally changes the migration properties of $nTiO_2$ in soil[10,11]. Therefore, this paper will explore the changes of surface Zeta potential of $nTiO_2$ under different environmental conditions and the effects of different environmental water flow velocities on its migration in phosphate environment.

1. Materials and methods

1.1 Preparation of the $nTiO_2$ phosphate suspension

All chemicals used in the experiment are analytical pure and purchased from Sinopharmgroup. 20 nm $nTiO_2$ was purchased from Shanghai Gaoquan Chemical Co., Ltd., 1 $g \cdot L^{-1}$ TiO_2 was weighed and dissolved in 0.1 mM phosphate solution (NaH_2PO_4) and 10 mM $NaNO_3$ electrolyte solution, and ultrasonic was used with an ultrasonic cleaner (KQ 2200B, ultrasonic instruments Co., Ltd., Hunshan, China) for 30 mins for migration experiment.

1.2 Test of the Zeta potential on the $nTiO_2$ particle surface

Accurately weigh 0.01 g of TiO_2 particles into a 100 mL beaker and prepare suspensions under different conditions. The different conditions are electrolyte $NaNO_3$ concentration (0.1–5 mM) and phosphate solution (0.1–5 mM), in which the pH value of all suspensions is adjusted to pH = 6.50 with diluted HCl and NaOH. Then, the suspension of $nTiO_2$ particles with adjusted pH value was placed on the ultrasonic instrument for 30 mins. After ultrasonic treatment, the suspension was placed on a stirrer and stirred for 30s. Finally, the Zeta potential of $nTiO_2$ particles was tested with Marvin Nano-ZS90. All samples were tested three times, and the average value was taken as the final Zeta potential value.

1.3 Migration experiment of quartz sand column

Referring to Fang, *et al.*, column leaching experiment was used to study the migration behavior of $nTiO_2$[2]. A chromatographic column with a length of 17.5 cm and an inner diameter of 25 mm was selected. The chromatographic column was filled with quartz sand and saturated with deionized water for 12 h. Inject 200 ml (10 mM $NaNO_3$) of background solution into the saturated chromatographic column with a peristaltic pump, and collect 10ml of effluent every 10 mins with an automatic sample partial collector (BS-100A, Huxi, Shanghai). Then, about 5 pore volumes (PV) of the $nTiO_2$ suspension were injected into the chromatographic column, and 20 tubes of effluent were collected with an automatic partial collector. After the suspension is injected, continue to inject 5 PV $NaNO_3$ background solution, collect the effluent and wait for test.

1.4 Analysis and determination of the titanium and phosphorus concentrations

Analysis and determination of titanium (TI): take 2 mL of $nTiO_2$ suspension and put it into a 25 mL beaker, add 1–2 mL of sulfuric acid ammonium sulfate digestion solution to the beaker, place it on a heating plate and heat it at 220 ℃ for 1–1.5 h. After digestion, transfer the solution to a 50 mL volumetric flask for constant volume, then transferring 5 mL into a 50 mL volumetric flask, and successively adding 8 mL ($V_{\text{hydrochloric acid}}$:$V_{\text{deionized water}}$ = 5:1) dilute hydrochloric acid, 2 ml (10 $g \cdot L^{-1}$) ascorbic acid and 10 mL diantipyrylmethane hydrochloride solution with constant volume. The concentration of Ti was measured with an ultraviolet spectrophotometer (TU-1901, Shimadzu, Japan) at a wavelength of 390 nm. Dilute 1000 $mg \cdot L^{-1}$ titanium standard stock solution (matrix is 0.15 $mol \cdot L^{-1}$ HNO_3) into a series of standard solutions (concentration gradient is 1–5 $mg \cdot L^{-1}$), and then obtain the standard curve and measure the concentration of titanium.

Analysis and determination of total phosphorus: determine the phosphorus concentration by molybdenum blue chromogenic method, put the solution to be measured into a 50 mL volumetric flask to volume, and successively add a drop of phenolphthalein, a drop of 1 $mol \cdot L^{-1}$ NaOH solution (shake well), a drop of 1 $mol \cdot L^{-1}$ sulfuric acid solution (shake well to colorless), 1 mL (100 $g \cdot L^{-1}$) anti chemical acid and 2 mL molybdate to volume[12]. After 20 mins of

color development, the absorbance of phosphorus (P) was measured with an ultraviolet spectrophotometer at the wavelength of 700 nm. In addition, dilute the phosphorus standard stock solution into a series of standard solutions with a concentration gradient of 1–5 mg·L^{-1}, measure the absorbance at the same wavelength, then obtain the standard curve and determine the phosphorus concentration.

Analysis and determination of dissolved phosphorus: take 5 mL of $nTiO_2$ suspension into 7 mL high-speed centrifuge tube, place the centrifuge tube in ultra-high-speed centrifuge (GL-21M, Thermo Fisher Technology Company), and centrifuge at 4 ℃ and 15,000 r·min^{-1} for 1 h. Pass the supernatant over 0.22 μM porous filter membrane, test the concentration of dissolved phosphorus according to the above method of testing total phosphorus.

1.5 A two-point kinetic model

A two-point kinetic adsorption model (TSKAM) was chosen with the equation[13,14].

$$\frac{\partial \theta C}{\partial t}+\rho_b \frac{\partial (S_1)}{\partial t}+\rho_b \frac{\partial (S_2)}{\partial t}=\frac{\partial}{\partial x}\left(\theta D \frac{\partial C}{\partial x}\right)-\frac{\partial vC}{\partial x} \quad (1)$$

Among them, θ is the porosity of the quartz sand column, and C represents the concentration of $nTiO_2$ particles in the solution, ρ_b represents the unit weight of quartz sand, x represents the spatial vertical coordinate axis, and D represents the hydraulic dispersion coefficient, v represents the water flow velocity, S_1 and S_2 represent $nTiO_2$ sites 1 and 2, respectively. The core of TSKAM model is to divide the sites on the quartz sand surface conducive to the adsorption of TiO_2 particles into site 1 and site 2. The $nTiO_2$ particles retained at site 2 are controlled by convection dispersion, and the mass conservation equation is the first-order kinetic adsorption and desorption equation.

$$\rho_b \frac{\partial (S_2)}{\partial t}=\theta k_2 C-\rho_b k_{2d} S_2 \quad (2)$$

k_2 and k_{2d} are the adsorption and desorption rates at site 2, respectively, and the adsorption of the $nTiO_2$ particles at site 2 belongs to the reversible adsorption. The mass conservation equation on site 1 is:

$$\rho_b \frac{\partial (S_1)}{\partial t}=\theta k_1 \psi_x C \quad (3)$$

k_1 is the adsorption rate at the colloidal site 1. Adsorption at site 1 is irreversible adsorption. ψ_x is a function related to the depth of the filled column[13].

$$\psi_x=\left(\frac{d_c+x-x_0}{d_c}\right)^{-\beta} \quad (4)$$

Where, d_c is the average particle size of quartz sand and x_0 is the distance on the coordinate axis. At this distance, the reten of $nTiO_2$ particles is related to the column depth. β is an empirical coefficient that controls the shape of the spatial $nTiO_2$ curve. The smaller the values of site 2 adsorption efficiency (k_2), analytical efficiency (k_{2d}) and site 1 adsorption efficiency (k_1) are, the less the reten $nTiO_2$ of particles on quartz sand and the higher their mobility will be. The penetration curve of $nTiO_2$ particles is simulated by HYDRUS-1d software to obtain parameters k_1, S_1, k_2 and k_{2d}[15].

1.6 Migration parameters

The $nTiO_2$ particle mass recovery can be obtained by performing area integration of its migration curves.

$$MR(\%)=\frac{\int_0^{\infty} Q(t)C(t)\mathrm{d}t}{\int_0^{t_0} Q(t)C_0(t)\mathrm{d}t} \quad (5)$$

In formula, Q is the pore flow velocity (mL·min^{-1}), C_0 and C are the inflow and outflow TiO_2 concentration (mg·L^{-1}), t is time (min) and t_0 is pulse duration (min).

The probability of $nTiO_2$ particles adsorbing on the quartz sand surface is called the adsorption efficiency (α).

$$\alpha=-\frac{2d_c}{3(1-\theta)L\eta^0}\ln\left(\frac{C}{C_0}\right) \quad (6)$$

In formula, L is the length of the column. θ is

the porosity of the filled column. d_c is the diameter of sand and η_0 is the theoretical single medium contact efficiency.

Net bed penetration coefficient:

$$\lambda_0=-\frac{1}{L}\ln\left(\frac{C}{C_0}\right) \quad (7)$$

Particulate deposition rate coefficient:

$$k=\lambda_0 \nu_p \quad (8)$$

In formula, v_p is the flow velocity and k is the coefficient of time and distance correlation.

The maximum migration distance of the nTiO2 particles was defined as the distance at which the nTiO2 particles move when 99.9% of the nTiO2 particles are trapped, that is,

$$L_{max}=-\frac{\nu_p}{\kappa}\ln\left(\frac{C}{C_0}\right) \quad (9)$$

The results of the various migration parameters for the above formula are shown in **Table 1**.

Table 1. Physical and computational parameters of $nTiO_2$ particles and quartz sand columns in the migration experiments

Number	$NaNO_3$ Concentrated/mM	P concentrated/mM	Flow speed/ ml· min^{-1}	Outflow ratio/%	Single medium contact efficiency	Adsorption efficiency	Adsorption efficiency/ cm^{-1}	Sedimentation rate coefficient/h^{-1}	Maximum migration distance/cm
1	10	0.1	0.5	3.9	35.9	3.56×10^{-4}	0.19	2.705	37.3
2	10	0.1	1	12	35.9	2.32×10^{-4}	0.12	3.536	57
3	10	0.1	2.5	38	35.9	1.06×10^{-4}	0.06	4.034	124.9

2. Results and discussion

2.1 Effect of different concentrations of $NaNO_3$ electrolytes on the Zeta potential on the $nTiO_2$ surface

When pH = 6.5, the change of surface Zeta potential of $nTiO_2$ in different concentrations of $NaNO_3$ is shown in **Figure 1(a)**. At different electrolyte concentrations, the Zeta potential on the surface of TiO_2 particles is negative, which indicates that the surface of TiO_2 particles is negatively charged at different concentrations of $NaNO_3$. With the increasing concentration of $NaNO_3$ in the solution, the Zeta potential on the surface of $nTiO_2$ particles decreases (the absolute value decreases, that is, the negative is getting smaller and smaller). When the $NaNO_3$ concentration increased from 0.1 mM to 5 mM, the corresponding Zeta potential changed from –19 mV to –6.09 mV. This is mainly because with the increasing solubility of $NaNO_3$ in the solution, the charge shielding effect and electrostatic double layer on the surface of $nTiO_2$ particles are compressed, and the net negative charge on the surface of TiO_2 particles decreases[16,17]. As a result, the Zeta potential on the

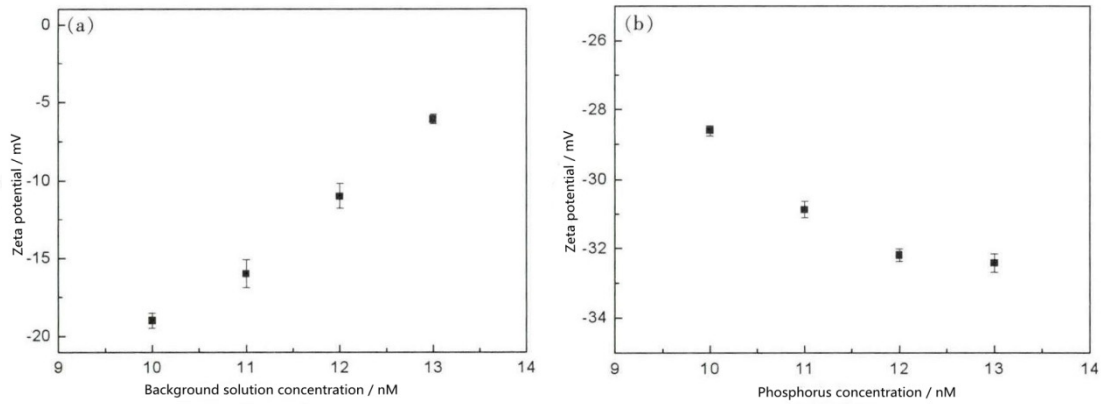

Figure 1. Zeta potentials of $nTiO_2$ particles with different $NaNO_3$ concentrations (a) and different phosphorus concentrations (b) in the 10 mM $NaNO_3$ background solution (pH = 6.5).

surface of $nTiO_2$ particles is reduced, so the dispersion stability of $nTiO_2$ particle suspension is also reduced.

2.2 Effect of different phosphorus concentrations on the Zeta potential on the $nTiO_2$ surface

As shown in **Figure 1(b)**, when pH = 6.5 and background solution $NaNO_3$ is 10 mM, the Zeta potential on the surface of $nTiO_2$ particles increases with the increase of P concentration. For example, when the P concentration is 0.1 mM, its surface Zeta potential is –28.6 mV, while when the P concentration is increased to 5 mM, its surface Zeta potential increases to –32.43 mV. The results show that because phosphate is adsorbed on the surface of $nTiO_2$ particles, the charge density on the surface of $nTiO_2$ particles is improved through the deprotonation of surface carboxyl groups[18]. Therefore, the electrostatic repulsion between the $nTiO_2$ particles and the $nTiO_2$ particles adsorbing P is strengthened, which eventually leads to the improvement of the dispersion stability of the $nTiO_2$ particle suspension[19].

2.3 Effect of water flow velocity on the migration of $nTiO_2$ particles suspended in a phosphate solution

The effects of different water flow velocities (0.5–2.5 $mL \cdot min^{-1}$) on the migration of TiO_2 particles and P in quartz sand column were investigated when the suspension pH was 6.5, the phosphate concentration was 0.1 mM and the background solution $NaNO_3$ concentration was 10 mM. The flow velocity selected in this group of experiments is within the range of groundwater flow velocity. **Figure 2** shows the penetration curve of $nTiO_2$ particles at different water velocities. With the increase of water flow velocity, the outflow ratio (C/C_0) of $nTiO_2$ particles increases continuously. When the water flow velocity increases from 0.5 $mL \cdot min^{-1}$ to 2.5 $mL \cdot min^{-1}$, the outflow ratio of $nTiO_2$ particles increases from 3.9% to about 38.0%, which is similar to the migration law of nano-hydroxyapatite in quartz sand column under different water flow velocities[21]. The above phenomenon is mainly because with the increase of water flow velocity in the quartz sand column, the total sites on the quartz sand surface that can be adsorbed by $nTiO_2$ particles in the quartz sand column also decrease. When the water flow velocity is very high, the total sites on the quartz sand surface that can be adsorbed by $nTiO_2$ particles decrease sharply due to the action of hydraulic shear force. The retention of $nTiO_2$ particles in quartz sand column also decreases. In addition, when the water flow velocity is very low, it is difficult to provide enough kinetic energy for $nTiO_2$ particles to penetrate the quartz sand column in the quartz sand column with small porosity, and a large number of $nTiO_2$ particles are retained in the quartz sand column[21–23].

In addition, it can be seen from **Table 1** that when the water flow rate increases from 0.5 $mL \cdot min^{-1}$ to 2.5 $mL \cdot min^{-1}$, the adsorption efficiency of $nTiO_2$ particles on the surface of quartz sand reduces from 3.56×10^{-4} to 1.06×10^{-4}, the retention of $nTiO_2$ particles in quartz sand column is reduced and the migration ability is continuously improved. Although the deposition rate coefficient increased from 2.705 h^{-1} to 7.699 h^{-1}, due to the increase of water flow velocity, the continuous improvement of hydraulic shear force improves continuously, the active collision increases continuously during migration, the retention of $nTiO_2$ particles on the surface of quartz sand decreased constantly, and more $nTiO_2$ particles penetrated the quartz sand column. In addition, the maximum migration distance of $nTiO_2$ particles is also increasing with the increase of water flow velocity, and the maximum migration distance is greater than the height of the column by 17.5 cm, which shows that $nTiO_2$ particles can smoothly penetrate the quartz sand column under these three different water flow velocities. Therefore, the increase of water flow velocity promotes the migration of $nTiO_2$ particles in the quartz sand column. As for the effect of water velocity on the migration of $nTiO_2$ particles in saturated quartz sand column, the two-point dynamic model can well simulate the penetration curve of $nTiO_2$ particles in quartz sand column. As shown in Table 2, the water flow velocity is 0.5–2.5 $mL \cdot min^{-1}$, and the simulated R^2 are 0.983, 0.996 and 0.990 respectively, indicating that the model has

high fitting degree. With the increase of water flow velocity, the adsorption efficiency of site 1 (k_1), site 2 (k_2) and the first-order desorption rate (k_{1d}) on site 1 decrease, which indicates that the adsorption of $nTiO_2$ particles on the surface of quartz sand is less, resulting in the increase of their migration, which is more conducive to their migration.

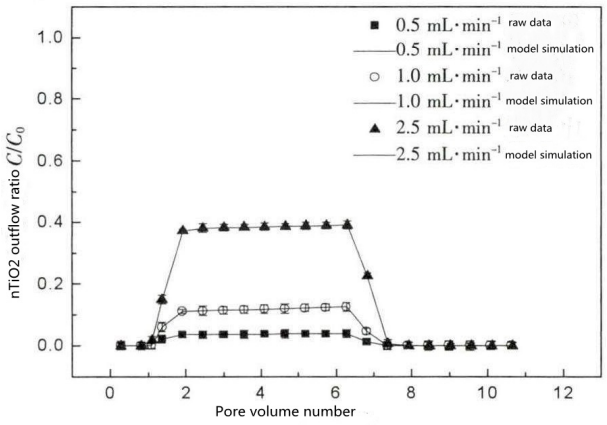

Figure 2. Penetration curve of $nTiO_2$ particles at different water flow speeds.

2.4 Effect of water flow velocity on phosphate migration

As shown in **Figure 3**, the outflow ratio of total P increases with the increase of water flow rate. When the water flow rate was 0.5 mL·min^{-1}, the outflow ratio of total P was 38.0%; When the flow rate increases to 1 mL·min^{-1}, the outflow ratio of total P is 50%. Continue to increase the flow rate to 2.5 mL·min^{-1}, and the outflow ratio of total P increases to 67.9%. This is mainly because with the increase of water flow velocity in the quartz sand column, the ability of $nTiO_2$ particles to penetrate the quartz sand column increases, so that the P adsorbed on the $nTiO_2$ particles also migrate out of the quartz sand column. After digestion, the measured total P concentration also increases. However, with the increase of water flow velocity, the outflow ratio of dissolved P does not change significantly, as shown in **Figure 4**. At this time, the outflow ratio of dissolved P is basically maintained at about 21.5%. There is no obvious change in the outflow ratio of dissolved P, mainly because the change of water flow velocity will not affect the adsorption capacity of $nTiO_2$ particles for P. Therefore, no matter how the water flow velocity changes, the concentration of dissolved P in the solution will not change. In addition, the dissolved P is obtained by subtracting the total phosphate from the bound P of $nTiO_2$ particles. Therefore, when the velocity is changed and the concentration of dissolved P remains unchanged, the water flow rate is at 0.5 mL·min^{-1}, the dissolved P in the effluent is the main, and only a small part of the bound P with $nTiO_2$ particles exists. When the water flow rate increases, most of the P in the effluent exists in the form of bound P with $nTiO_2$ particles, and only a small part exists in the form of dissolved P.

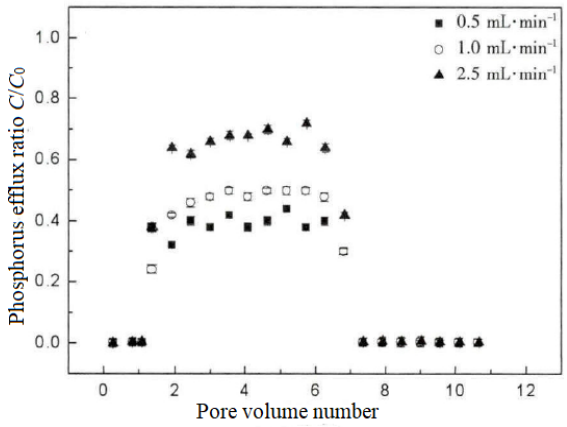

Figure 3. Penetration curves of total phosphorus suspended in (0.1 mM) phosphate solution at different flow rates.

Table 2. Simulation parameters of two-point kinetic adsorption model under different experimental conditions

Number	Site 2 adsorption efficiency	Site 2 resolution efficiency	Maximum value of retention at point 1	Site 1 adsorption efficiency	Person mean square correction factor
1	14.470	6.271	97.15	0.230	0.983
2	14.160	6.028	45.67	1.152	0.996
3	3.138	1.224	33.50	0.067	0.990

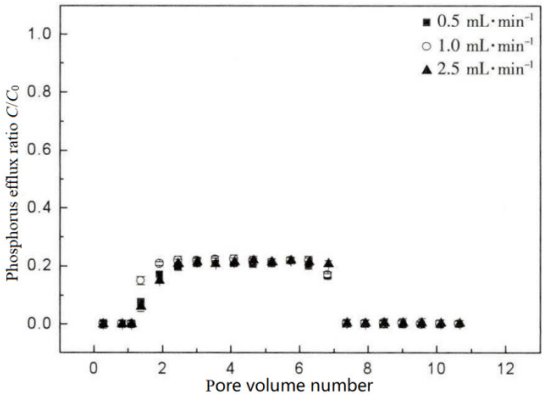

Figure 4. Penetration curves of dissolved phosphorus suspended in (0.1 mM) phosphate solution by different flow velocities.

3. Conclusion

(1) When pH = 6.5, with the increase of electrolyte $NaNO_3$ concentration, the Zeta negative potential on the surface of $nTiO_2$ particles decreased gradually; (2) The surface negative charge of $nTiO_2$ increases with the increase of P concentration, and its dispersion stability also improves constantly; (3) High flow velocity promotes the mobility of $nTiO_2$, and the migration of soluble phosphate also increases continuously; (4) The two-point kinetic adsorption model can well simulate the migration and penetration curve of nano materials in quartz sand column. The model results show that with the increase of flow rate, the adsorption efficiency of site 2 (k_2), analytical efficiency (k_{2d}) and site 1 adsorption efficiency (k_1) decrease, and the adsorption efficiency of $nTiO_2$ particles on quartz sand decreases, so that more $nTiO_2$ particles penetrate the quartz sand column.

Conflict of interest

The authors declare that they have no conflict of interest.

Acknowledgements

General Research Project of National Natural Science Foundation of China, No. 21377090.

References

1. Fang J, Shan X, Wen B, *et al.* Stability of titania nanoparticles in soil suspensions and transport in saturated homogeneous soil columns. Environmental Pollution 2009; 157(4): 110–109.
2. Higashi MM, Jardim WF. Remediation of pesticide contaminated soil using TiO_2, mediated by solar light. Catalysis Today 2002; 76(2-4): 201–207.
3. Nagaveni K, Sivalingam G, Hegde MS, *et al.* Photocatalytic degradation of organic compounds over combustion-synthesized nano-TiO_2. Environmental Science & Technology 2004; 38(5): 1600–1604.
4. Quan X, Zhao X, Chen S, *et al.* Enhancement of p, p'-DDT photodegradation on soil surfaces using TiO_2 induced by UV-light. Chemosphere 2005; 60(2): 266–273.
5. And TA, Madras G. Photocatalytic degradation of rhodamine dyes with nano-TiO_2. Industrial & Engineering Chemistry Research 2007; 46(1): 1–7.
6. Wei J, Hamid M, Baoshan X. Bacterial toxicity comparison between nano- and micro-scaled oxide particles. Environmental Pollution 2009; 157(5): 1619–1625.
7. Hund-Rinke K, Simon M. Ecotoxic effect of photocatalytic active nanoparticles (TiO_2) on algae and daphnids. Environmental Science & Pollution Research 2006; 13(4): 225–232.
8. Saleh N, Kim H, Phenrat T, *et al.* Ionic strength and composition affect the mobility of surface-modified FeO nanoparticles in water-saturated sand columns. Environmental Science & Technology 2008; 42(9): 3349–3355.
9. French RA, Jacoboson AR, Bojeong K, *et al.* Influence of ionic strength, pH, and cation valence on aggregation kinetics of titanium dioxide nanoparticles. Environmental Science & Technology 2009; 43(5): 1354–1359.
10. Healy KE, Ducheyne P. Hydration and preferential molecular adsorption on titanium in vitro. Biomaterials 1992; 13(8): 553–561.
11. Kaushik RD, Gupta VK, Singh JP. Distribution of zinc, cadmium, and copper forms in soils as influenced by phosphorus application. Arid Soil Research & Rehabilitation 2009; 7(2): 163–171.
12. Chen J, Gao F, Sun X. Determination of phosphorus content in alcoholic by molybdenum blue extraction photometric method. Chemical Engineer 2005; 115(4): 29–30.

13. Schijyen JF, Simunek J. Kinetic modeling of virus transport at the field scale. Journal of Contaminant Hydrology 2002; 55(1-2): 113–135.
14. Bradford SA, Simunek J, Bettahar M, *et al.* Modeling colloid attachment, straining, and exclusion in saturated porous media. Environmental Science & Technology 2003; 37(10): 2242–2250.
15. Marquardt DW. An algorithm for least-squares estimation of nonlinear parameters. Journal of the Society for Industrial & Applied Mathematics 2006; 11(2): 431–441.
16. Elimelech M, Gregory J, Jia X, *et al.* Particle deposition and aggregation：Measurement modeling and simulation. Woburn: BuaerworthHeinemann; 1995.
17. Hunter RJ. Foundations of colloid science. New York: Oxford University Press; 1987.
18. Solovitch N, Labille J, Rose J, *et al.* Concurrent aggregation and deposition of TiO_2 nanoparticles in a sandy porous media. Environmental Science & Technology 2010; 44(13): 4897–4902.
19. Pelley AJ, Tufenkji N. Effect of particle size and natural organic matter on the migration of nano- and microscale latex particles in saturated porous media. Journal of Colloid & Interface Science 2008; 321(1): 74–83.
20. Wang D, Bradford SA, Paradelo M, *et al.* Facilitated transport of copper with hydroxyapatite nanoparticles in saturated sand. Soil Science Society of America Journal 2012; 76(2): 375–388.
21. Gargiulo G, Bradford SA, Simunek J, *et al.* Transport and deposition of metabolically active and stationary phase deinococcus radiodurans in unsaturated porous media. Environmental Science & Technology 2007; 41(4): 1265–1271.
22. Gargiulo G, Bradford SA, Simunek J, *et al.* Bacteria transport and deposition under unsaturated flow conditions: The role of water content and bacteria surface hydrophobicity. Vadose Zone Journal 2008; 7(2): 406–419.
23. Bradford SA, Torkzaban S, Wiegmann A. Pore-scale simulations to determine the applied hydrodynamic torque and colloid immobilization. Vadose Zone Journal 2010; 10(1): 252–261.